Macromolecules

Article

pubs.acs.org/Macromolecules

# Morphology Evolution of PS-*b*-P2VP Diblock Copolymers via Supramolecular Assembly of Hydroxylated Gold Nanoparticles

Se Gyu Jang,[†] Anzar Khan,[‡] Craig J. Hawker,*[,†,§,⊥] and Edward J. Kramer*[,†,§,∥]

[†]Materials Research Laboratory, University of California, Santa Barbara, California, 93106, United States

[‡]Department of Materials, ETH-Zürich, CH-8093 Zürich, Switzerland

[§]Department of Materials, University of California, Santa Barbara, California, 93106, United States

[⊥]Department of Chemistry and Biochemistry, University of California, Santa Barbara, California, 93106, United States

[∥]Department of Chemical Engineering, University of California, Santa Barbara, California, 93106, United States

Supporting Information

**ABSTRACT:** We report on the strong segregation of core−shell Au nanoparticles, with a shell layer consisting of a random copolymer brush of styrene and vinylphenol (PS-*r*-PVPh-SH), in poly(styrene-*b*-2-vinylpyridine) (PS-*b*-P2VP) diblock copolymer. Because of the formation of multiple hydrogen bonds between the hydroxyl groups within the shell of the nanoparticles and the pyridine group in PS-*b*-P2VP, the Au nanoparticles were strongly localized into P2VP domains with a very high volume fraction of nanoparticles ($\phi_p \sim 0.53$). The spatial distribution of Au nanoparticles, observed by transmission electron microscopy (TEM), is compared with results of previous experiments where homopolymers were blended with block copolymers. If the diameter $d$ of the nanoparticles is much less than the width $D$ of the P2VP lamellar domains, these nanoparticles are more uniformly distributed across the P2VP domain than if $d$ is comparable to $D$, in which case the nanoparticles are pushed toward the center of the P2VP domains. This behavior is similar to that observed when homopolymers are blended with block copolymers. Novel morphological transitions from spherical to cylindrical P2VP morphologies and from lamellae to cylindrical PS morphologies were observed during coassembly of these functional nanoparticles with block copolymers.

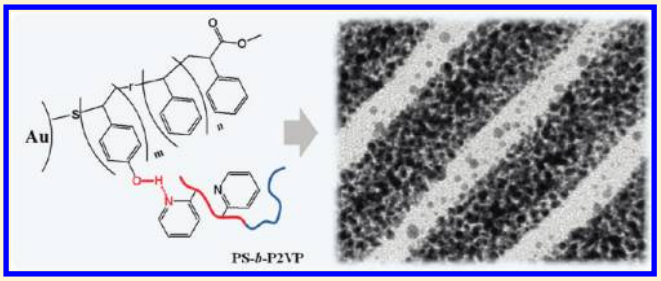


## INTRODUCTION

Hydrogen bonding (H-bonding) has been widely used for supramolecular assembly of small molecules and polymers because of its molecularly specific and highly directional characteristics.[1−4] In addition, the reversible and dynamic characteristics of H-bonding enable production of self-healing materials, which is an exciting emerging theme in materials science.[5−7] In particular, block copolymers constructed using multiple H-bonding units instead of covalent linkages have been studied intensively, both theoretically and experimentally.[8−14] A judicious choice of polymers, balancing polymer interactions with the strength and directionality of H-bonding groups, opens up possibilities to create complex structures with various properties derived from simple building blocks.[4,15] Demonstrations of these possibilities include low temperature processing of materials with well-defined architectures, thermal modulation of microphase-separated domains, and development of nonconventional morphologies with nanometer-scale features such as lamellae-in-lamellae and square arrangement of cylinders.[16−19] Recently, H-bonding has also been employed to blend block copolymers and homopolymers.[20−23] The formation of multiple H-bonds between host and guest polymers significantly enhances miscibility causing swelling of the host domains of the block copolymers without macrophase separation and corresponding order−order morphology transitions.

The incorporation of inorganic nanoparticles into block copolymer matrices has been intensively studied with the aim of combining the unique physical or chemical properties of nanoparticles with hierarchical nanophase-separated self-assembly of block copolymer, which is potentially useful in high performance catalysis, sensors, optics, and electronics.[24−28] Tailoring the surface properties of nanoparticles can provide for precise control of nanoparticle segregation in block copolymers. This control has been demonstrated using nanoparticles with short aliphatic chains, homopolymers, mixed homopolymers, and random copolymers.[29−44] It is known that nanoparticles completely covered by polymeric ligands show segregation behavior similar to that of the homopolymer in blending systems.[45−52] For example, nanoparticles covered with a polystyrene (PS) homopolymer brush layer tend to segregate in PS domains of poly(styrene-*b*-2-vinylpyridine) (PS-*b*-P2VP)

**Received:** October 26, 2011
**Revised:** December 20, 2011
**Published:** January 20, 2012

   dx.doi.org/10.1021/ma202391k | *Macromolecules* 2012, 45, 1553−1561

diblock copolymer at low particle volume fractions. However when higher volume fractions of such particles are added, they macrophase-separate due to an increase in the entropic penalty of block copolymer chain stretching resulting from nanoparticle incorporation.[35,38,53] Most characteristic features of homopolymer addition in blending systems such as swelling of domains, morphological transitions of block copolymer, and macrophase separation of additives were observed in coassembly of nanoparticles and block copolymers. In particular, a strong segregation of nanoparticles into specific domains via H-bonding has also been reported. For example, localization of nanoparticles of cadmium selenide (CdS), Au, and silicon (Si) covered with hydroxyl groups has been observed in the poly(ethylene oxide) (PEO) or poly(4-vinylpyridine) (P4VP) domains of diblock copolymers.[54−57] Because of the strong enthalphic attraction of H-bonds, macrophase-separation of nanoparticles was significantly suppressed in favor of microphase separation and very high volume fraction of nanoparticle incorporation (~36 vol %) was demonstrated.[55] Despite the similarity between polymer blend and nanoparticle incorporation systems, according to our best knowledge, no investigation correlating these two systems in detail have been reported. Combining knowledge from both systems may allow general predictions of segregation behavior for new sets of nanoparticles or homopolymers in block copolymer matrices in order to create customized and multifunctional hybrid materials.

In this paper, Au nanoparticles covered with a brush layer of thiol-terminated random copolymers of styrene and vinylphenol (PS-*r*-PVPh-SH) were prepared and the H-bonding attraction between the hydroxyl groups on the nanoparticle ligands and pyridine rings of PS-*b*-P2VP diblock copolymers studied. The PS-*r*-PVPh-SH ligands were synthesized by reversible addition−fragmentation transfer (RAFT) polymerization of styrene and 4-acetoxystyrene (PS-*r*-PAS-RAFT) followed by hydrazinolysis to deprotect the phenol groups and to generate a thiol group at the chain end. By controlling the relative number of *p*-vinylphenol to styrene units, solubility of Au nanoparticles in nonpolar solvents could be tuned to maximize the H-bonding strength. As a result, preparation of nanoparticle/block copolymer mixtures and solvent annealing could be carried out in nonpolar solvents without any disruption or weakening of H-bonds by solvation of the phenol units by polar solvents. The random copolymer-coated nanoparticles were strongly segregated in P2VP domains of PS-*b*-P2VP block copolymer of various molecular weights and 2VP mole fractions. The spatial distribution of the nanoparticles in P2VP domains of block copolymer were compared to results of previous experiments where homopolymers were blended with block copolymers. The high incorporation of homogeneously distributed nanoparticles into P2VP domains induced morphological transitions of the PS-*b*-P2VP diblock copolymers.

## EXPERIMENTAL METHODS

**Synthesis of PS-*r*-PAS-RAFT by RAFT Polymerization.** Thiol-terminated random copolymers of styrene and 4-acetoxystyrene (PS-*r*-PAS-RAFT) were synthesized via reversible addition−fragmentation transfer (RAFT) polymerization.[58,59] Dithioester-RAFT agent was prepared by the procedure described elsewhere.[34] Two PS-*r*-PAS-RAFTs were synthesized with different compositions. Styrene (Sigma-Aldrich, > 99%) and 4-acetoxystyrene (Sigma-Aldrich, 96%) were purified by passage through a basic aluminum oxide column prior to use. Styrene (6.02 g, 55.80 mmol), 4-acetoxystyrene (1.01 g, 6.20 mmol), azobis(isobutyronitrile) (AIBN, 0.01 g, 0.06 mmol), and dithioester RAFT agent (0.30 g, 0.62 mmol) were mixed and degassed by three freeze−pump−thaw cycles. The polymerization was carried out at 90 °C for 7 h under vacuum. The polymer was then precipitated in methanol and dried under vacuum. The molecular weight ($M_n$) and polydispersity index (PDI) of the random copolymer $PS_{22}$-*r*-$PAS_3$-RAFT as measured by gel permeation chromatography (GPC, calibrated by PS standards), were 2.6 kg/mol and 1.1, respectively. The composition of PS-*r*-PAS-RAFT calculated from $^1$H NMR was found to be 12 mol % 4-acetoxystyrene (~3 repeating units). The $M_n$ value of $PS_{22}$-*r*-$PAS_3$-RAFT calculated from the ratio of the peak area of RAFT agent to that of PS (broad peaks from 6.2 to 7.3 ppm) and acetoxy groups (broad peak centered at 2.3 ppm) was 3.3 kg/mol. Following the same procedure, a PS-*r*-PAS-RAFT with 26 mol % 4-acetoxystyrene (~7 repeating units, $PS_{20}$-*r*-$PAS_7$-RAFT) was synthesized. The $M_n$ and PDI for this copolymer were 2.7 kg/mol (3.7 kg/mol by $^1$H NMR) and 1.1, respectively.

**Deprotection of PS-*r*-PAS-RAFT.** The dithioester-terminus and acetoxy groups of the PS-*r*-PAS-RAFT were converted to thiol and hydroxyl groups, respectively, in a one step reaction by hydrazinolysis as reported by Lee et al.[60] PS-*r*-PAS-RAFT (1.0 g) was placed in a round-bottom flask with a magnetic stirrer. Dry THF (30 mL) was transferred into the flask via a cannula after three vacuum and argon purging cycles. Under a dry argon atmosphere, 15 mmol of hydrazine dissolved in THF (Sigma-Aldrich, 1M, 50 equiv. to dithioester-terminus) was injected by syringe (***Caution!*** *hydrazine is highly toxic and should be handled with extreme care*). The solution color changed from pink to yellow immediately. After the reaction was stirred overnight, the solvent and hydrazine were evaporated and the polymers were dissolved in dichloromethane, filtered with a syringe filter (Whatman, 200 nm pore size, PTFE) to remove insoluble species, and precipitated in cold hexane. The precipitated white polymers were dried under vacuum at room temperature for a day.

**Synthesis of PS-*r*-PVPh-SH-Coated Au Nanoparticles (PS-*r*-PVPh−S-Au).** Au nanoparticles coated with PS-*r*-PVPh-SH were synthesized using the THF one-phase method.[61] Au precursor ($HAuCl_4{\cdot}3H_2O$, Sigma-Aldrich, > 99.9%, 0.8 mmol) and 0.2 mmol of $PS_{22}$-*r*-$PVPh_3$-SH or $PS_{20}$-*r*-$PVPh_7$-SH polymers were placed in a round-bottom flask with a magnetic stirrer. Dry THF (20 mL) was transferred into the flask via a cannula under agitation after three vacuum and argon purging cycles. After stirring for 30 min, Au nanoparticles were synthesized by adding 2.3 mmol of the reducing agent, superhydride ($Li(C_2H_5)_3BH$, Sigma-Aldrich, 1 M in THF), dropwise under dry argon. The unbound polymer ligands were separated from the polymer brush coated Au nanoparticles by filtering, at least 5 times, with membrane centrifugal filters (Centricon-Plus 70, MWCO 100 000 Da, Millipore Inc.) using THF as the solvent. The washed Au nanoparticles in THF were filtered with a syringe filter (Whatman, 200 nm, PTFE) and precipitated in hexane.

**Preparation of PS-*b*-P2VP/Au Nanoparticle Composites.** A certain weight of Au nanoparticles was dissolved in a freshly prepared 1 wt % PS-*b*-P2VP diblock copolymer solution in dichloromethane (DCM) to obtain a volume fraction of nanoparticles in the range of 0.04−0.53. This volume fraction includes the volume of the polymer shell estimated from the density of the ligand (~1.05 g/cm$^3$) and Au (~19.3 g/cm$^3$) coupled with thermal gravimetric analysis (TGA) of the Au nanoparticles.[35] P2VP sphere-forming (107 kg/mol with a mole fraction of 2VP, $f_{P2VP} \sim 0.11$) and lamellae-forming (72 kg/mol with $f_{P2VP} \sim 0.40$ and 199 kg/mol with $f_{P2VP} \sim 0.48$) PS-*b*-P2VP block copolymers were used for the preparation of composites. Thick films of block copolymers and block copolymer/nanoparticle composites were prepared by drop casting the solution of nanoparticles and PS-*b*-P2VP block copolymer in DCM onto a thick Au-coated (~100 nm) sodium chloride crystal window (Sigma-Aldrich, 2 mm thick). The composites were annealed in saturated dichloromethane (DCM) vapor at room temperature for at least 2 days. After drying the composite film overnight under vacuum, a thick Au layer (~100 nm) was deposited on the sample to inhibit infiltration of the epoxy resin (Embed-812, Electron Microscopy Sciences) into the sample during TEM sample preparation. Samples of the composite film were

Scheme 1. Schematic Illustration of Synthesis of Thiol-Terminated Poly(styrene-*ran*-vinyl phenol) Copolymer Ligand[a]

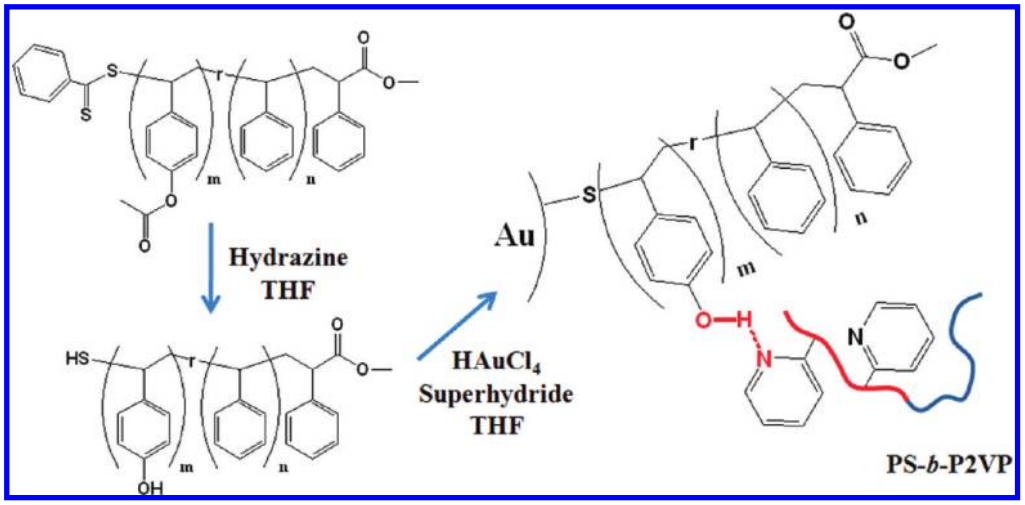


[a]This was performed by hydrazinolysis of poly(styrene-*ran*-acetoxystyrene) obtained by reversible addition fragmentation chain transfer (RAFT) polymerization and hydrogen bond formation between hydroxyl groups in ligands coated on Au nanoparticles and pyridine groups on poly(styrene-*b*-2-vinylpyridine) diblock copolymer. The hydrolysis of acetoxy groups and the reduction of dithio-ester groups were carried out simultaneously by addition of hydrazine with tetrahydrofurane (THF) as a solvent. Gold nanoparticles were synthesized by reduction of chloroauric acid trihydrate with superhydride ($Li(C_2H_5)_3BH$) in the presence of random copolymer ligands dissolved in THF.

embedded into epoxy resin and sliced to a thickness of about 50−70 nm by ultramicrotoming (Leica). The sliced composite samples were exposed to iodine vapor to selectively stain the P2VP domains.

**Characterization.** The nanoparticles and cross-sections of the pure block copolymers and composite films were characterized by transmission electron microscopy (TEM, FEI Tecnai G2 microscope, 200 kV). The size histograms of the Au nanoparticles were determined from at least 300 nanoparticles by image analysis (Image Pro) of TEM micrographs. The mean areal chain density of polymer ligands on the Au nanoparticles was calculated from the total surface area and the weight fraction of Au and polymer ligands determined by TGA. Fourier transform infrared (FT-IR, Bruker) spectra of PS-*b*-P2VP diblock copolymer and composite samples were taken in the wavenumber range of 450−4000 $cm^{-1}$.

## RESULTS AND DISCUSSION

Scheme 1 illustrates the strategy for synthesis of Au nanoparticles coated with random copolymer ligands containing phenolic groups and their supramolecular assembly with the pyridine groups of a poly(styrene-*b*-2-vinylpyridine) (PS-*b*-P2VP) diblock copolymer. Thiol-terminated poly(styrene-*r*-vinylphenol) (PS-*r*-PVPh-SH) ligands are obtained from the random copolymer of poly(styrene-*r*-acetoxystyrene) synthesized by reversible addition−fragmentation chain transfer (RAFT) polymerization (PS-*r*-PAS-RAFT). The hydrolysis of acetoxy groups and the reduction of thioester groups to a secondary thiol were carried out simultaneously by addition of hydrazine.[60] Then, Au nanoparticles covered with PS-*r*-PVPh-SH ligands were synthesized by reduction of a Au precursor ($HAuCl_4 \cdot 3H_2O$) with superhydride ($Li(C_2H_5)_3BH$) dissolved in THF. A key to the design of the nanoparticles is tailoring the surface properties of the polymeric shell by controlling the number of phenolic groups per polymeric ligand with enough hydroxyl groups being present to induce a strong H-bonding interaction. At the same time, the number of hydroxyl groups needs to be low enough to maintain reasonable hydrophobicity, enabling dissolution of the nanoparticles in nonpolar solvents such as dichloromethane. This avoids the need to use polar solvents, which weaken the H-bonding interaction with the P2VP by solvation of the PVPh.[20] The enthalpic gain from H-bond formation attracts the nanoparticles to the P2VP phase of microphase-separated PS-*b*-P2VP diblock copolymer domains. However the enthalpic penalty due to mixing of PS components of the polymer shell of the nanoparticles with the P2VP phase drives the nanoparticles to the PS phase. Therefore, the number ratio of styrene and phenol repeating units on the ligand determines the segregation location of nanoparticles in PS-*b*-P2VP domains as well as the solubility of nanoparticles in nonpolar solvents. To broadly define an optimum ratio, we synthesized two PS-*r*-PAS-RAFT polymers with different numbers of repeating units; $PS_{22}$-*r*-$PAS_3$-RAFT and $PS_{20}$-*r*-$PAS_7$-RAFT as shown in Table 1 (see Supporting Information, Figure S1, for $^1H$ NMR spectra of each polymer).

Table 1. Characterization of Poly(styrene-*r*-acetoxy styrene) Synthesized by RAFT Polymerization

| | GPC | | $^1H$ NMR[a] | | |
|---|---|---|---|---|---|
| | $M_n$ (kg/mol) | PDI | $M_n$ (kg/mol) | $N_S$[b] | $N_{AS}$[c] |
| $PS_{22}$-*r*-$PAS_3$-RAFT | 2.6 | 1.1 | 3.3 | 22 | 3 |
| $PS_{20}$-*r*-$PAS_7$-RAFT | 2.7 | 1.1 | 3.7 | 20 | 7 |

[a]Calculated from the ratio of the peak area of RAFT agent to that of PS (broad peaks from 6.2 to 7.3 ppm) and acetoxy groups (broad peak centered at 2.3 ppm) by $^1H$ NMR. [b]Average number of styrene repeating units per chain obtained by $^1H$ NMR. [c]Average number of acetoxy styrene repeating units per chain obtained by $^1H$ NMR.

The hydrazinolysis of the random copolymers was monitored by $^1H$ NMR (Figure 1). Figure 1a shows the $^1H$ NMR spectrum of the $PS_{22}$-*r*-$PAS_3$-RAFT ($CDCl_3$) with the aromatic protons of the dithioester end group at a chemical shift of 7.8 ppm and methyl protons of the acetoxy groups at 2.3 ppm (marked by the inverse triangle), respectively.[60] After hydrazinolysis, these two peaks disappeared and a new broad peak at 9.0 ppm, corresponding to the phenolic protons, was observed (marked by the inverse triangle, Figure 1b, DMSO-$d_6$). This observation indicates that both the reduction of the dithioester group to a secondary thiol and hydrolysis of


dx.doi.org/10.1021/ma202391k | *Macromolecules* 2012, 45, 1553−1561

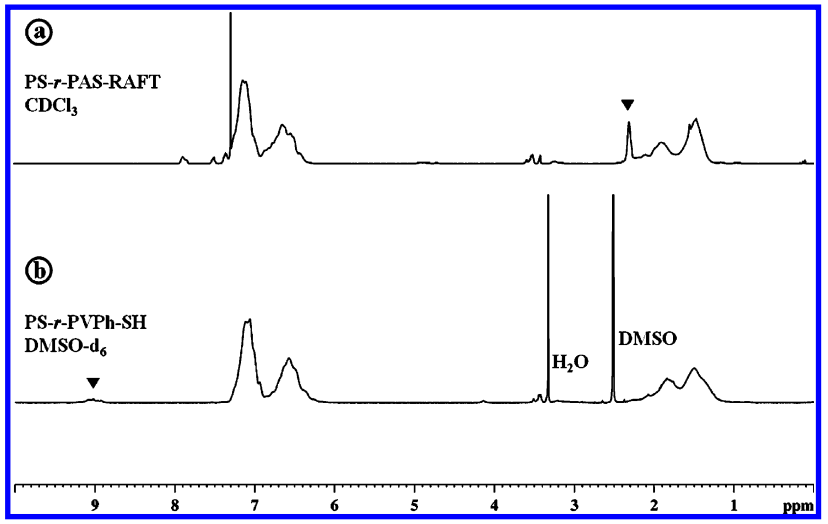


**Figure 1.** $^1$H NMR spectra of a) poly(styrene-*ran*-acetoxystyrene) ($PS_{22}$-*r*-$PAS_3$-RAFT, $CDCl_3$) and b) thiol-terminated poly(styrene-*ran*-vinylphenol) ($PS_{22}$-*r*-$PVPh_3$-SH, DMSO-$d_6$) after hydrolysis of acetoxy groups and reduction of dithioester groups.

acetoxystyrene units to phenols are completed simultaneously by hydrazinolysis. The resulting $PS_{22}$-*r*-$PVPh_3$-SH copolymer was highly soluble in dichloromethane and toluene. On the other hand, the $PS_{20}$-*r*-$PVPh_7$-SH copolymer showed good solubility only in polar solvents such as THF and dimethylformamide. The synthesis of Au nanoparticles with $PS_{22}$-*r*-$PVPh_3$-SH copolymer ligands via the Brüst two-phase method, using toluene/water mixture, resulted in aggregated nanoparticles during the reduction of the Au precursor, maybe due to amphiphilicity of the random $PS_{22}$-*r*-$PVPh_3$-SH copolymer ligand. In contrast, synthesis of Au nanoparticles via the one-phase method in THF, under an argon atmosphere, was successful with no aggregated nanoparticles being observed for either copolymer. As expected, the Au nanoparticles covered with $PS_{22}$-*r*-$PVPh_3$-SH ($PS_{22}$-*r*-$PVPh_3$-S-Au) and $PS_{20}$-*r*-$PVPh_7$-SH ($PS_{20}$-*r*-$PVPh_7$—S-Au) ligands showed different solubility with the $PS_{22}$-*r*-$PVPh_3$-S-Au nanoparticles having high solubility in nonpolar solvents such as dichloromethane and toluene and the $PS_{20}$-*r*-$PVPh_7$—S-Au nanoparticles showing only limited solubility in the same solvents (about 2 mg/mL in dichloromethane).

Characterization of the $PS_{22}$-*r*-$PVPh_3$-S-Au nanoparticles by transmission electron microscopy (TEM) revealed their relatively narrow size distribution (histogram in the inset, see Supporting Information, Figure S2, for TEM image and size distribution of $PS_{20}$-*r*-$PVPh_7$—S-Au nanoparticles) with the average core diameter of the nanoparticles ($d_{core}$) being 3.4 ± 1.6 nm and the areal chain density of ligands on the nanoparticle surface ($\Sigma$), 1.0/nm$^2$ (Figure 2a). Similarly, characterization of the neat sphere-forming PS-*b*-P2VP diblock copolymer (107 kg/mol, with a mole fraction of 2VP units $f_{P2VP} \sim 0.11$) annealed in saturated dichloromethane vapor for 2 days shows regular spherical P2VP domains as dark spheres as a result of staining with iodine vapor (Figure 2b). Significantly, after adding a small volume fraction $\phi_p \sim 0.06$ of $PS_{22}$-*r*-$PVPh_3$-S-Au nanoparticles and solvent annealing in DCM, the nanoparticles in the PS-*b*-P2VP diblock copolymer were strongly segregated into the spherical P2VP domains as seen in Figures 2c,d. This strong segregation is due to the formation of multiple H-bonds between the large number of hydroxyl groups on the nanoparticle ligands and the pyridine rings of the 2VP units. There are about 145 phenolic hydroxyl groups per nanoparticle on average based on the number of ligands on each nanoparticle surface (see Supporting Information, Figure S3, characterized through a series of FT-IR spectra revealing multiple H-bonding formation). Synthesis of Au nanoparticles with thiol-terminated poly(styrene-*r*-acetoxystyrene) (PS-*r*-PAS-SH) ligands and investigation of their segregation behavior in PS-*b*-P2VP diblock copolymer domains are desirable as a control to further confirm the influence of hydrogen bonding on the segregation of nanoparticle. However, the synthesis of Au nanoparticles with PS-*r*-PAS-SH ligands is challenging due to difficulty in selective reduction of dithioester group without deprotection of the acetoxy groups along the backbone (see Supporting Information, Figure S4, showing deprotection of acetoxy group during reduction of dithioester and nanoparticle synthesis with superhydride). Synthesis of random copolymer ligands with polystyrene and *p*-methoxystyrene (PS-*r*-PMS-RAFT) may be an alternative way to avoid the formation of phenol group during synthesis of ligand and nanoparticles. However, the segregation behavior of the nanoparticles with PS-*r*-PMS-SH ligands cannot be directly compared to the nanoparticles with PS-*r*-PAS-SH.

A further increase in $\phi_p$ to 0.16 resulting in an increase in $\phi_{P+P2VP}$ to 0.24 and in the formation of disordered cylindrical P2VP domains (Figure 2e) with no macrophase separation of the nanoparticles from the diblock copolymer domains (Figure 2f). The morphology transition from spherical to cylindrical P2VP indicates that the Au nanoparticles have effects similar to those of a homopolymer with H-bonding donors, as demonstrated by Dobrosielska and Matsushita in the model system PS-*b*-P2VP and poly(4-hydroxystyrene).[21,22] However, the disordered cylindrical phases (Figures 1e,f) are novel and have not been observed when homopolymers are added to block copolymers. This new behavior may be due to the jamming of nanoparticles at high incorporation in the P2VP domains, such jamming of particles located at interface is known to induce metastable morphologies in the cases of immiscible polymer blends or immiscible liquids.[32,62−64]

The spatial distribution of homopolymer chains in block copolymer domains, which can control the morphology of block copolymer/homopolymer blends, is highly dependent on the relative size ratio of the block copolymer and the


dx.doi.org/10.1021/ma202391k | *Macromolecules* 2012, 45, 1553−1561

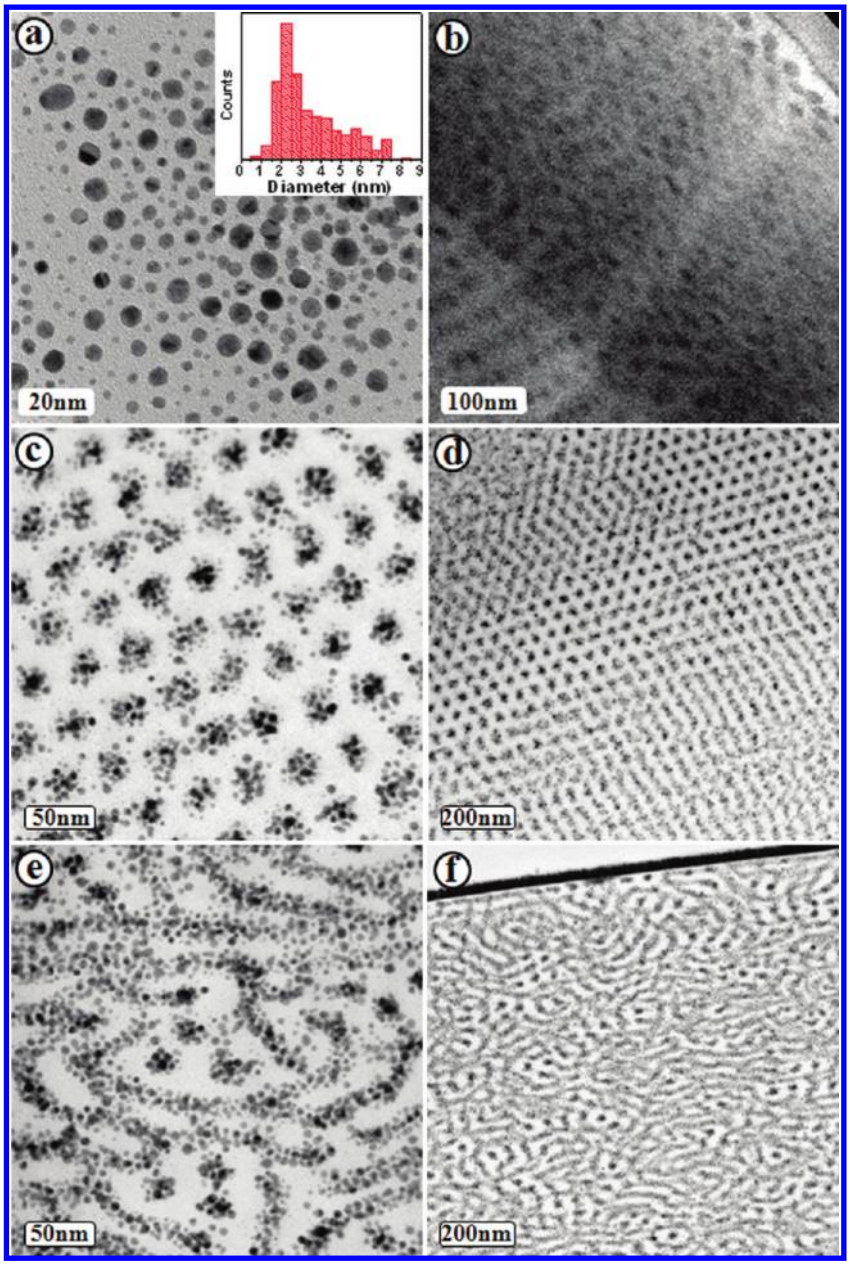


**Figure 2.** TEM micrographs of Au nanoparticles covered with PS-*r*-PVPh-SH ligands ($PS_{22}$-*r*-$PVPh_3$-S-Au) and their segregation in sphere-forming PS-*b*-P2VP diblock copolymer. (a) TEM micrograph of $PS_{22}$-*r*-$PVPh_3$-S-Au nanoparticles and a histogram showing their size distribution obtained from more than 300 nanoparticles by image analysis. Average diameter of nanoparticles ($d_{core}$) is 3.4 ± 1.6 nm. Areal chain density of ligands is ~1.0/$nm^2$. (b) Cross-sectional TEM micrograph of PS-*b*-P2VP diblock copolymer (107 kg/mol, $f_{P2VP} \sim 0.11$) annealed in saturated dichloromethane vapor for 2 days. P2VP domains stained by iodine vapor appear as black spheres. (c–f) Cross-sectional TEM micrographs of PS-*b*-P2VP/nanoparticle composites. The $PS_{22}$-*r*-$PVPh_3$-S-Au nanoparticles appearing as small black dots were strongly segregated into the spherical P2VP domains (c and d). Further increases in the volume fraction of nanoparticles ($\phi_p$) resulted in the formation of disordered P2VP cylinders (e and f). A dark film on the top of the composite film in part f is a Au film deposited during the sample preparation for microsectioning to protect the composite sample from swelling by epoxy resin. $\phi_p$ values of c, d and e, f are 0.06 and 0.16, respectively.

homopolymer.[49−51] Homopolymers with significantly lower molecular weight than that of the host block of the block copolymer are distributed uniformly, which results in both uniform expansion of chemical junctions of block copolymer and the morphology transitions expected as the volume fraction of the host block and homopolymer increases. In contrast, homopolymers with higher molecular weight segregate to the center of the corresponding domains or are macrophase-separated. The same behavior has been observed from blending of diblock copolymer and homopolymers that have H-bonding interactions.[21,22] In order to characterize the distribution of homopolymers in such blends, small-angle X-ray scattering (SAXS) can be employed to track changes in domain spacing of block copolymer but offers only indirect evidence for the location of the homopolymer additive. An outstanding advantage of using nanoparticles instead of homopolymer is the inherent visibility of nanoparticles through TEM imaging allowing the distribution of nanoparticle additives within the block copolymer domains to be determined as shown in Figure 3. Parts a and b of Figure 3 are cross-sectional TEM


dx.doi.org/10.1021/ma202391k | *Macromolecules* 2012, 45, 1553−1561

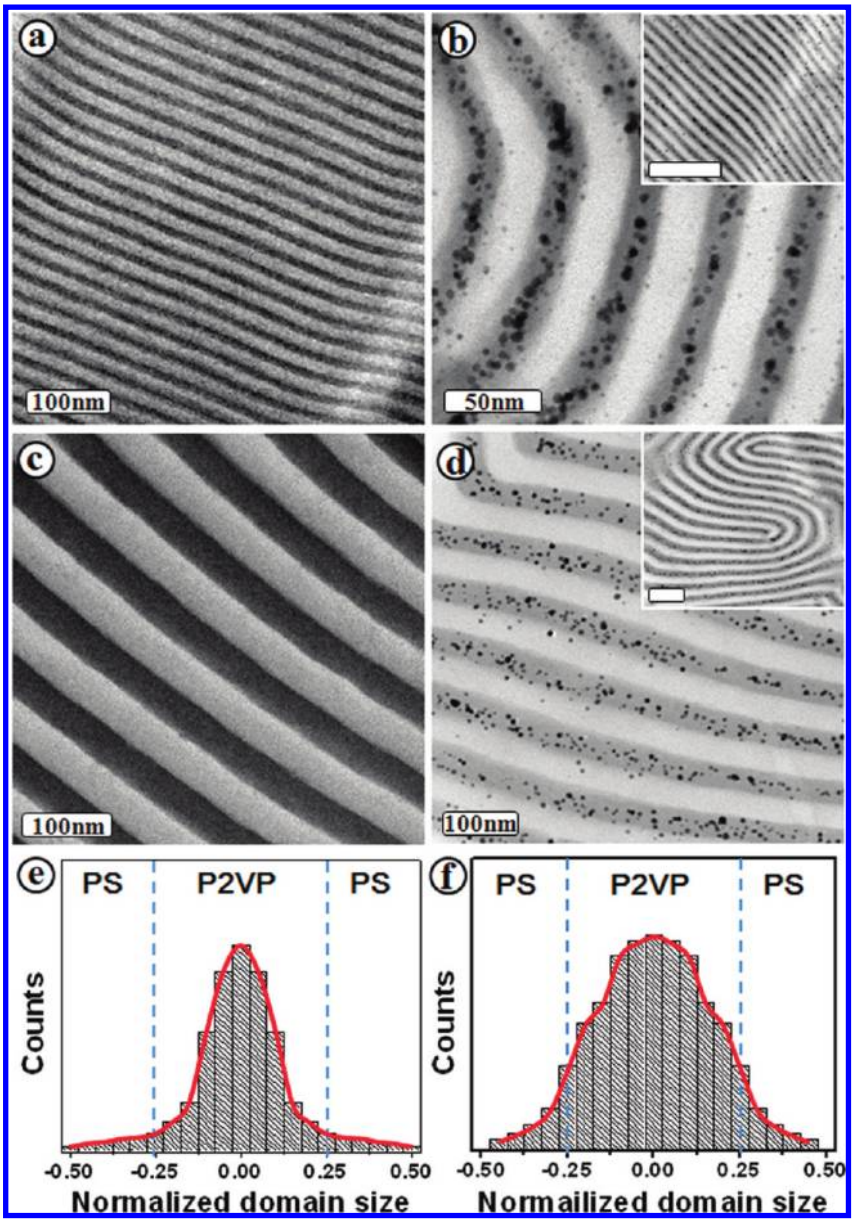


**Figure 3.** Cross-sectional TEM micrographs of lamellar PS-*b*-P2VP diblock copolymer: (a) 72 kg/mol ($f_{P2VP} \sim 0.40$) and (b) its composite with $PS_{22}$-*r*-$PVPh_3$-S-Au nanoparticles ($\phi_p \sim 0.04$). Cross-sectional TEM micrographs of lamellar PS-*b*-P2VP diblock copolymer (c) 199 kg/mol ($f_{P2VP} \sim 0.48$) and its composite with $PS_{22}$-*r*-$PVPh_3$-S-Au nanoparticles ($\phi_p \sim 0.04$). Inset images show lower magnification TEM micrographs of each sample. Histograms in parts e and f display the distribution of $PS_{22}$-*r*-$PVPh_3$-S-Au nanoparticles in the diblock copolymers shown in b and d, respectively. The normalized domain size refers to the distance of the nanoparticle from the center of the P2VP domain divided by the size of a single period of the structure formed by PS-*b*-P2VP. The blue dotted lines located at +0.25 and −0.25 represent the interfaces between PS and P2VP. $PS_{22}$-*r*-$PVPh_3$-S-Au nanoparticles were partially aggregated at the center of P2VP domains as shown in parts b and *e*. Meanwhile, the same nanoparticles were more homogeneously distributed in P2VP domains with larger molecular weight (d and f). Scale bars in the insets are 200 nm.

micrographs of PS-*b*-P2VP diblock copolymer (72 kg/mol, $f_{P2VP} \sim 0.40$) without and with $PS_{22}$-*r*-$PVPh_3$-S-Au nanoparticles, respectively. The lamellar morphology of the diblock copolymer in Figure 3a was preserved on the addition of $PS_{22}$-*r*-$PVPh_3$-S-Au nanoparticles with $\phi_p \sim 0.04$ (Figure 3b). Although some $PS_{22}$-*r*-$PVPh_3$-S-Au nanoparticles were observed in PS domains, a histogram in Figure 3e, obtained from image analysis of Figure 3b, clearly shows that most nanoparticles were segregated at the center of P2VP domains. This indicates that the size of $PS_{22}$-*r*-$PVPh_3$-S-Au nanoparticles, including polymeric ligands ($d_{core+ligand} \sim 6.8 \pm 2.2$ nm), is too large to be homogeneously distributed in P2VP domains having the comparable average equilibrium domain thickness measured from Figure 3a ($D_{P2VP,0} \sim 10$ nm). The average domain thickness of P2VP with $PS_{22}$-*r*-$PVPh_3$-S-Au nanoparticles ($D_{P2VP+P}$) in Figure 3b was significantly greater than the $D_{P2VP,0}$ in Figure 3a ($D_{P2VP+P}/D_{P2VP,0} \sim 1.5$), due to the confinement of nanoparticles at the center of P2VP domains and their corresponding expansion. Meanwhile, the domain thickness of PS remained the same upon addition of nanoparticles ($D_{PS}/D_{PS,0} \sim 1$), indicating that there is no expansion of the area per block copolymer chemical junction which would induce a morphology transition.[22,23,49] Interestingly, the same nanoparticles with $\phi_p \sim 0.04$ were more uniformly distributed in P2VP domains of a higher molecular weight PS-*b*-P2VP diblock copolymer (199 kg/mol, $f_{P2VP} \sim$


dx.doi.org/10.1021/ma202391k | *Macromolecules* 2012, 45, 1553−1561

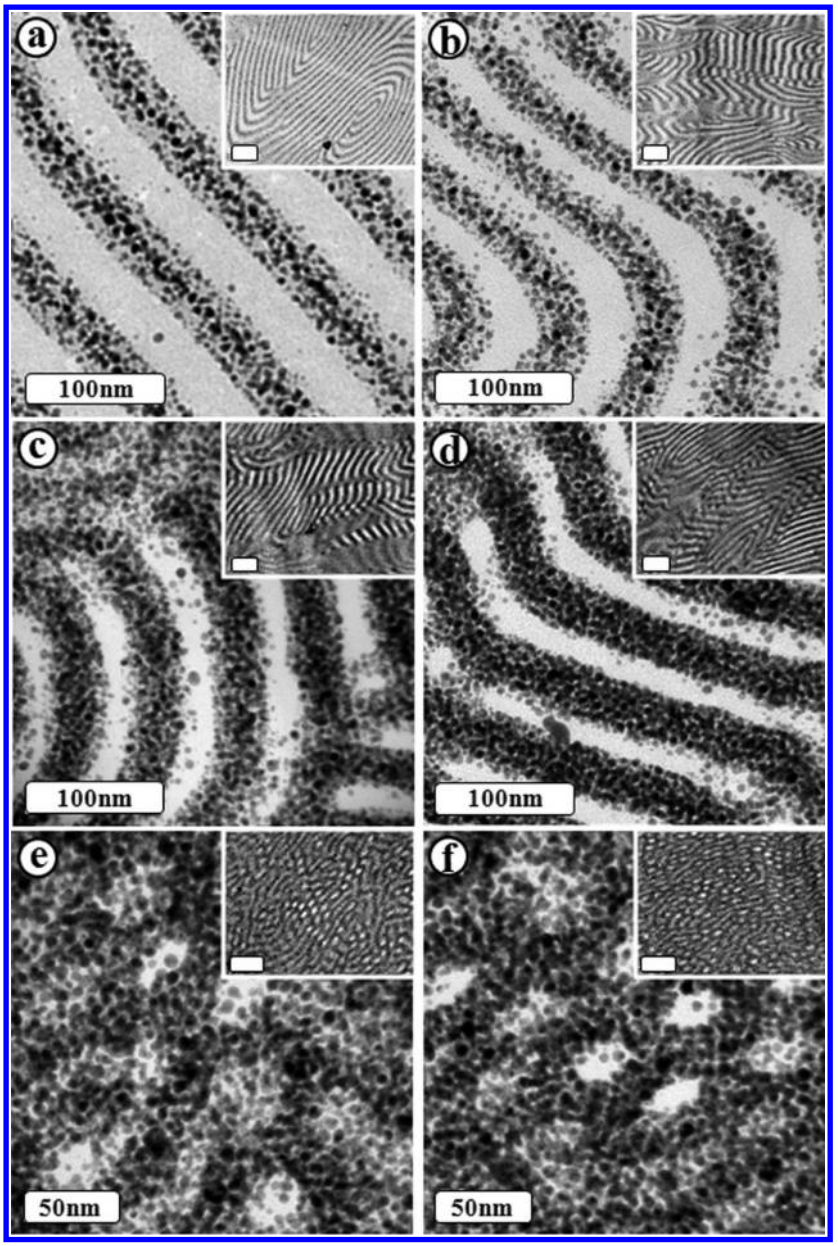


**Figure 4.** Cross-sectional TEM micrographs of lamellar PS-*b*-P2VP diblock copolymer (199 kg/mol, $f_{P2VP} \sim 0.48$) with various volume fractions of $PS_{22}$-*r*-$PVPh_3$-S-Au nanoparticles $\phi_p$: (a) 0.08, (b) 0.16, (c) 0.21, (d) 0.32, (e) 0.42, and (f) 0.53. Inset images show a corresponding lower magnification TEM micrographs of each sample. Scale bars in the insets are 200 nm. The decrease in PS domain thickness by segregated nanoparticles is observed resulting from the increase in $\phi_p$. The transition from lamellar to cylindrical PS was observed at $\phi_p \sim 0.32$. Calculated volume fractions of P2VP, including the volume of the nanoparticles, $\phi_{P+P2VP}$ are (a) 0.52, (b) 0.56, (c) 0.59, (d) 0.65, (e) 0.70, and (f) 0.76.

0.48, $M_{nP2VP} \sim 96$ kg/mol) as shown in the TEM micrograph (Figure 3d) and the histogram (Figure 3f). A decrease in average thickness of PS domains was observed upon addition of nanoparticles ($D_{PS}/D_{PS,0} \sim 0.8$) due to the expansion of chemical junctions of block copolymer chains at the interface and the corresponding relaxation of the stretched conformation of the PS chains. These results agree qualitatively with the observations from homopolymer/block copolymer blending experiments.

The decrease in average thickness for the PS domain upon addition of the $PS_{22}$-*r*-$PVPh_3$-S-Au nanoparticles demonstrates that morphology transitions for PS-*b*-P2VP diblock copolymer are possible by further increasing $\phi_{P+P2VP,}$ similar to that observed for uniformly distributed homopolymer in a diblock copolymer. Figure 4 shows a series of cross-sectional TEM micrographs of the PS-*b*-P2VP diblock copolymer (199 kg/mol, $f_{P2VP} \sim 0.48$) with various volume fractions ($\phi_p$) ranging from 0.08 to 0.53 of $PS_{22}$-*r*-$PVPh_3$-S-Au nanoparticles including the volume of the ligands. Volume fraction values of the gold core on a ligand-free basis ($\phi_{P,\,core}$) for each samples in Figure 4, are (a) 0.02, (b) 0.03, (c) 0.04, (d) 0.06, (e) 0.09, and (f) 0.11. The $PS_{22}$-*r*-$PVPh_3$-S-Au nanoparticles are closely packed in P2VP domains regardless of $\phi_p$, with no macrophase separation from block copolymer domains. The calculated volume fractions of P2VP domains, including the volume of the nanoparticles ($\phi_{P+P2VP}$), are (a) 0.52, (b) 0.56, (c) 0.59, (d) 0.65, (e) 0.70, and (f) 0.76. As $\phi_{P+P2VP}$ increases, the lamellar structure was distorted more significantly (Figures 4a–c), and a morphological transition from one that is lamellar to one with PS cylinders was observed at $\phi_{P+P2VP} \sim 0.65$ (Figures 4d and


dx.doi.org/10.1021/ma202391k | *Macromolecules* 2012, 45, 1553–1561

4e). The long-range order of block copolymer domains was gradually suppressed upon increasing $\phi_{P+P2VP}$, and finally a disordered PS cylindrical morphology was developed (Figure 4f). The variation of normalized lamellar domain thickness ($D/D_0$), which is the ratio of average PS (or P2VP) domain thickness $D$, at a volume fraction $\phi_p$, to the average domain thickness $D_0$ for $\phi_p = 0$, is plotted versus the nanoparticle volume fraction $\phi_p$ in Figure 5. As reported for the polymer blend system,[23,49] the average domain thickness of PS was dramatically reduced compared to the original thickness without nanoparticle addition ($D/D_0 \sim 0.4$ at $\phi_p \sim 0.32$). Meanwhile, in contrast to the polymer blend cases that show significant swelling of the domains containing the homopolymer, the normalized domain thickness of P2VP was only slightly increased upon addition of nanoparticles. This slight increase in P2VP domain thickness may be due to the nonequilibrium structure of PS-*b*-P2VP as a result of nanoparticle jamming or due to a change in P2VP chain conformation filling the interstitial voids around the densely packed nanoparticles.

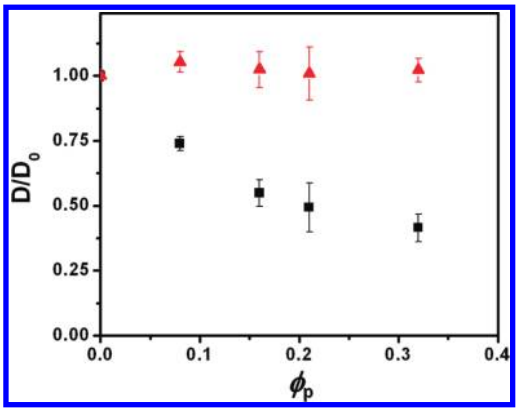


**Figure 5.** Normalized lamellar domain thickness ($D/D_0$) of PS (black squares) and P2VP (red triangles) versus the volume fraction of nanoparticles $\phi_p$. The normalized domain thickness of PS decreased dramatically from the original thickness without addition of nanoparticles ($D/D_0 \sim 0.4$). Meanwhile, the average domain thickness of P2VP was slightly increased. Domain thicknesses were measured by TEM image analysis of Figures 3c and 4a–d. For accurate measurements, the samples were tilted to align the direction of the lamellar planes and electron beam of the microscope to reduce the broadening of interfaces caused by misalignment of the electron beam.

## CONCLUSION

Au nanoparticles covered by PS-*r*-PVPh-SH ligands were designed to offer tunable supramolecular interactions through control of the number of phenolic groups while at the same time affording good solubility in nonpolar solvent via the styrenic repeat units. Through this design, H-bonding interactions with pyridine groups in PS-*b*-P2VP diblock copolymers can be maximized. The resulting $PS_{22}$-*r*-$PVPh_3$-S-Au nanoparticles showed high solubility in nonpolar solvents and strong segregation into P2VP domains while allowed a dramatic increase in the volume fraction of nanoparticles ($\phi_p \sim 0.53$) that could be blended without macrophase separation. The nanoparticles confined at the center of P2VP domains and the corresponding swelling of P2VP domains were clearly observed by TEM in the low molecular weight diblock copolymer (72 kg/mol, $f_{P2VP} \sim 0.40$). In contrast, the same nanoparticles were more homogeneously distributed in P2VP domains of a larger molecular weight diblock copolymer (199 kg/mol, $f_{P2VP} \sim 0.48$). Novel morphological transitions from spherical or lamellar to disordered cylindrical morphologies were observed as a result of strong segregation of nanoparticles into P2VP domains. These results clearly demonstrate the opportunities for nanoparticles with various functional cores (magnetic, catalytic, or fluorescent) to produce multifunctional composite materials with hierarchical nanostructures and high nanoparticle loading.

## ASSOCIATED CONTENT

### Supporting Information

$^1$H NMR spectra of $PS_{22}$-*r*-$PAS_3$-RAFT and $PS_{20}$-*r*-$PAS_7$-RAFT (Figure S1), TEM micrograph and size distribution of $PS_{20}$-*r*-$PVPh_7$–S-Au nanoparticles (Figure S2), FT-IR spectra revealing the formation of multiple H-bonding in composite (Figure S3), and $^1$H NMR spectra showing deprotection of acetoxy groups during reduction of dithioester and nanoparticle synthesis with superhydride and cross-sectional TEM micrograph of Au–S–$PAS_{1.7}$-*r*-$PVPh_{1.3}$-*r*-$PS_{22}$ nanoparticles in PS-*b*-P2VP microdomains (Figure S4). This material is available free of charge via the Internet at http://pubs.acs.org.

## AUTHOR INFORMATION

### Corresponding Author

*(C.J.H.) Telephone: 805-893-7161. Fax 805-893-8797. E-mail: hawker@mrl.ucsb.edu. (E.J.K.) Telephone: 805-893-4999. Fax: 805-893-8486. E-mail: edkramer@mrl.ucsb.edu.

## ACKNOWLEDGMENTS

This work was supported by the MRSEC Program of the National Science Foundation (NSF) under Award DMR11-21053. Materials Research Laboratory Central Facilities are supported by the MRSEC Program of the NSF under Award DMR11-21053; a member of the NSF-funded Materials Research Facilities Network (www.mrfn.org).

## REFERENCES

(1) Warren, S. C.; Messina, L. C.; Slaughter, L. S.; Kamperman, M.; Zhou, Q.; Gruner, S. M.; DiSalvo, F. J.; Wiesner, U. *Science* **2008**, *320*, 1748–1752.

(2) (a) Boyer, C.; Stenzel, M. H.; Davis, T. P. *J. Polym. Sci., Polym. Chem.* **2011**, *49*, 551–595. (b) Foster, E. J.; Berda, E. B.; Meijer, E. W. *J. Polym. Sci., Polym. Chem.* **2011**, *49*, 118–126. (c) Celiz, A. D.; Scherman, O. A. *J. Polym. Sci., Polym. Chem.* **2010**, *48*, 5833–5841. (d) Kurzhals, S.; Binder, W. H. *J. Polym. Sci., Polym. Chem.* **2010**, *48*, 5522–5532.

(3) Binder, W. H.; Zirbs, R. *Adv. Polym. Sci.* **2007**, *207*, 1–78.

(4) Zhao, Y.; Thorkelsson, K.; Mastroianni, A. J.; Schilling, T.; Luther, J. M.; Rancatore, B. J.; Matsunaga, K.; Jinnai, H.; Wu, Y.; Poulsen, D.; Frechet, J. M. J.; Alivisatos, A. P.; Xu, T. *Nat. Mat* **2009**, *8*, 979–985.

(5) Wojtecki, R. J.; Meador, M. A.; Rowan, S. J. *Nat. Mat.* **2011**, *10*, 14–27.

(6) Blaiszik, B. J.; Kramer, S. L. B.; Olugebefola, S. C.; Moore, J. S.; Sottos, N. R.; White, S. R. *Annu. Rev. Mat. Res.* **2010**, *40*, 79–211.

(7) Cordier, P.; Tournilhac, F.; Soulie-Ziakovic, C.; Leibler, L. *Nature* **2008**, *451*, 977–980.

(8) Feng, E. H.; Lee, W. B.; Fredrickson, G. H. *Macromolecules* **2007**, *40*, 693–702.

(9) Huh, J.; ten Brinke, G. *J. Chem. Phys.* **1998**, *109*, 789–797.

(10) Binder, W. H.; Bernstorff, S.; Kluger, C.; Petraru, L.; Kunz, M. J. *Adv. Mater.* **2005**, *17*, 2824–2828.

(11) Lee, W. B.; Elliott, R.; Katsov, K.; Fredrickson, G. H. *Macromolecules* **2007**, *40*, 8445−8454.
(12) Yang, X. W.; Hua, F. J.; Yamato, K.; Ruckenstein, E.; Gong, B.; Kim, W.; Ryu, C. Y. *Angew. Chem., Int. Ed.* **2004**, *43*, 6471−6474.
(13) Feldman, K. E.; Kade, M. J.; de Greef, T. F. A.; Meijer, E. W.; Kramer, E. J.; Hawker, C. J. *Macromolecules* **2008**, *41*, 4694−4700.
(14) Feldman, K. E.; Kade, M. J.; Meijer, E. W.; Hawker, C. J.; Kramer, E. J. *Macromolecules* **2010**, *43*, 5121−5127.
(15) Ruokolainen, J.; Makinen, R.; Torkkeli, M.; Makela, T.; Serimaa, R.; ten Brinke, G.; Ikkala, O. *Science* **1998**, *280*, 557−560.
(16) Ruokolainen, J.; Saariaho, M.; Ikkala, O.; ten Brinke, G.; Thomas, E. L.; Torkkeli, M.; Serimaa, R. *Macromolecules* **1999**, *32*, 1152−1158.
(17) Tang, C. B.; Lennon, E. M.; Fredrickson, G. H.; Kramer, E. J.; Hawker, C. J. *Science* **2008**, *322*, 429−432.
(18) Noro, A.; Matsushita, Y.; Lodge, T. P. *Macromolecules* **2008**, *41*, 5839−5844.
(19) Noro, A.; Matsushita, Y.; Lodge, T. P. *Macromolecules* **2009**, *42*, 5802−5810.
(20) Dobrosielska, K.; Takano, A.; Matsushita, Y. *Macromolecules* **2010**, *43*, 1101−1107.
(21) Dobrosielska, K.; Wakao, S.; Takano, A.; Matsushita, Y. *Macromolecules* **2008**, *41*, 7695−7698.
(22) Dobrosielska, K.; Wakao, S.; Suzuki, J.; Noda, K.; Takano, A.; Matsushita, Y. *Macromolecules* **2009**, *42*, 7098−7102.
(23) (a) Chen, S. C.; Kuo, S. W.; Jeng, U. S.; Su, C. J.; Chang, F. C. *Macromolecules* **2010**, *43*, 1083−1092. (b) Tirumala, V. R.; Romang, A.; Agarwal, S.; Lin, E. K.; Watkins, J. J. *Adv. Mater.* **2008**, *20*, 1603−1608. (c) Tirumala, V. R.; Daga, V.; Bosse, A. W.; Romang, A.; Ilavsky, J.; Lin, E. K.; Watkins, J. J. *Macromolecuels* **2008**, *41*, 7978−7985.
(24) Bockstaller, M. R.; Thomas, E. L. *J. Phys. Chem. B* **2003**, *107*, 10017−10024.
(25) Cheng, J. Y.; Ross, C. A.; Chan, V. Z. H.; Thomas, E. L.; Lammertink, R. G. H.; Vancso, G. J. *Adv. Mater.* **2001**, *13*, 1174−1178.
(26) Jaramillo, T. F.; Baeck, S. H.; Cuenya, B. R.; McFarland, E. W. *J. Am. Chem. Soc.* **2003**, *125*, 7148−7149.
(27) Mui, S. C.; Trapa, P. E.; Huang, B.; Soo, P. P.; Lozow, M. I.; Wang, T. C.; Cohen, R. E.; Mansour, A. N.; Mukerjee, S.; Mayes, A. M.; Sadoway, D. R. *J. Electrochem. Soc.* **2002**, *149*, A1610−A1615.
(28) Jang, S. G.; Khan, A.; Dimitriou, M. D.; Kim, B. J.; Lynd, N. A.; Kramer, E. J.; Hawker, C. J. *Soft Matter* **2011**, *7*, 6255−6263.
(29) Bockstaller, M. R.; Thomas, E. L. *Phys. Rev. Lett.* **2004**, *93*, 166106.
(30) Chiu, J. J.; Kim, B. J.; Kramer, E. J.; Pine, D. J. *J. Am. Chem. Soc.* **2005**, *127*, 5036−5037.
(31) Chiu, J. J.; Kim, B. J.; Yi, G. R.; Bang, J.; Kramer, E. J.; Pine, D. J. *Macromolecules* **2007**, *40*, 3361−3365.
(32) Chung, H.; Ohno, K.; Fukuda, T.; Composto, R. J. *Nano Lett.* **2005**, *5*, 1878−1882.
(33) (a) Kang, H.; Detcheverry, F. A.; Mangham, A. N.; Stoykovich, M. P.; Daoulas, K. C.; Hamers, R. J.; Muller, M.; de Pablo, J. J.; Nealey, P. F. *Phys. Rev. Lett.* **2008**, *100*, 148303. (b) Kuila, B. K.; Rama, M. S.; Stamm, M. *Adv. Mater.* **2011**, *23*, 1797−1800. (c) Daga, V. K.; Watkins, J. J. *Macromolecules* **2010**, *43*, 9990−9997. (d) Daga, V. K.; Anderson, E. R.; Gido, S. P.; Watkins, J. J. *Macromolecules* **2011**, *44*, 6793−6799. (e) Sary, N.; Richard, F.; Brochon, C.; Leclerc, N.; Leveque, P.; Audinot, J. N.; Berson, S.; Heiser, T.; Hadziioannou, G.; Mezzenga, R. *Adv. Mater.* **2010**, *22*, 763−768.
(34) Kim, B. J.; Bang, J.; Hawker, C. J.; Chiu, J. J.; Pine, D. J.; Jang, S. G.; Yang, S. M.; Kramer, E. J. *Langmuir* **2007**, *23*, 12693−12703.
(35) Kim, B. J.; Bang, J.; Hawker, C. J.; Kramer, E. J. *Macromolecules* **2006**, *39*, 4108−4114.
(36) Kim, B. J.; Chiu, J. J.; Yi, G. R.; Pine, D. J.; Kramer, E. J. *Adv. Mater.* **2005**, *17*, 2618−2622.
(37) Kim, B. J.; Fredrickson, G. H.; Hawker, C. J.; Kramer, E. J. *Langmuir* **2007**, *23*, 7804−7809.
(38) Kim, B. J.; Fredrickson, G. H.; Kramer, E. J. *Macromolecules* **2008**, *41*, 436−447.
(39) Park, S. C.; Kim, B. J.; Hawker, C. J.; Kramer, E. J.; Bang, J.; Ha, J. S. *Macromolecules* **2007**, *40*, 8119−8124.
(40) Kim, J.; Green, P. F. *Macromolecules* **2010**, *43*, 10452−10456.
(41) Hickey, R. J.; Sanchez-Gaytan, B. L.; Cui, W. H.; Composto, R. J.; Fryd, M.; Wayland, B. B.; Park, S. J. *Small* **2010**, *6*, 48−51.
(42) Costanzo, P. J.; Beyer, F. L. *Macromolecules* **2007**, *40*, 3996−4001.
(43) Böker, A.; Lin, Y.; Chiapperini, K.; Horowitz, R.; Thompson, M.; Carreon, V.; Xu, T.; Abetz, C.; Skaff, H.; Dinsmore, A. D.; Emrick, T.; Russell, T. P. *Nat. Mat.* **2004**, *3*, 302−306.
(44) Hu, Y. X.; Chen, D. A.; Park, S.; Emrick, T.; Russell, T. P. *Adv. Mater.* **2010**, *22*, 2583−2587.
(45) Bockstaller, M. R.; Mickiewicz, R. A.; Thomas, E. L. *Adv. Mater.* **2005**, *17*, 1331−1349.
(46) Balazs, A. C.; Emrick, T.; Russell, T. P. *Science* **2006**, *314*, 1107−1110.
(47) Huh, J.; Ginzburg, V. V.; Balazs, A. C. *Macromolecules* **2000**, *33*, 8085−8096.
(48) Tanaka, H.; Hasegawa, H.; Hashimoto, T. *Macromolecules* **1991**, *24*, 240−251.
(49) Hashimoto, T.; Tanaka, H.; Hasegawa, H. *Macromolecules* **1990**, *23*, 4378−4386.
(50) Semenov, A. N. *Macromolecules* **1993**, *26*, 2273−2281.
(51) Torikai, N.; Takabayashi, N.; Noda, I.; Koizumi, S.; Morii, Y.; Matsushita, Y. *Macromolecules* **1997**, *30*, 5698−5703.
(52) Mayes, A. M.; Russell, T. P.; Satija, S. K.; Majkrzak, C. F. *Macromolecules* **1992**, *25*, 6523−6531.
(53) Kim, B. J.; Fredrickson, G. H.; Bang, J.; Hawker, C. J.; Kramer, E. J. *Macromolecules* **2009**, *42*, 6193−6201.
(54) Yeh, S. W.; Chang, Y. T.; Chou, C. H.; Wei, K. H. *Macromol. Rapid Commun.* **2004**, *25*, 1680−1686.
(55) Lin, Y.; Daga, V. K.; Anderson, E. R.; Gido, S. P.; Watkins, J. J. *J. Am. Chem. Soc.* **2011**, *133*, 6513−6516.
(56) Li, Q. F.; He, J. B.; Glogowski, E.; Li, X. F.; Wang, J.; Emrick, T.; Russell, T. P. *Adv. Mater.* **2008**, *20*, 1462−1466.
(57) Yeh, S. W.; Wei, K. H.; Sun, Y. S.; Jeng, U. S.; Liang, K. S. *Macromolecules* **2003**, *36*, 7903−7907.
(58) Drockenmuller, E.; Li, L. Y. T.; Ryu, D. Y.; Harth, E.; Russell, T. P.; Kim, H. C.; Hawker, C. J. *J. Polym. Sci., Polym. Chem.* **2005**, *43*, 1028−1037.
(59) Perrier, S.; Takolpuckdee, P. *J. Polym. Sci., Polym. Chem.* **2005**, *43*, 5347−5393.
(60) Lee, C. U.; Roy, D.; Sumerlin, B. S.; Dadmun, M. D. *Polymer* **2010**, *51*, 1244−1251.
(61) Yee, C. K.; Jordan, R.; Ulman, A.; White, H.; King, A.; Rafailovich, M.; Sokolov, J. *Langmuir* **1999**, *15*, 3486−3491.
(62) Cates, M. E.; Clegg, P. S. *Soft Matter* **2008**, *4*, 2132−2138.
(63) Herzig, E. M.; White, K. A.; Schofield, A. B.; Poon, W. C. K.; Clegg, P. S. *Nat. Mat.* **2007**, *6*, 966−971.
(64) Stratford, K.; Adhikari, R.; Pagonabarraga, I.; Desplat, J. C.; Cates, M. E. *Science* **2005**, *309*, 2198−2201.